**Eurasian Journal of Physics and Functional Materials**

**2026, 10(2), 121-136**

# Calibration and Performance of the ENGREN Scintillation Array for Prompt Fission Neutron Spectrometry

Sh.S. Zeynalov[1], O.V. Sidorova[1,2,*], D.B. Berikov[1,3], A.I. Madadzada[1,4], S.M. Nuruyev[1,5], G.S. Ahmadov[1,4,5,6]

[1]Joint Institute for Nuclear Researches, Dubna, Russia

[2]Dubna State University, Dubna, Russia

[3]Institute of Nuclear Physics, Almaty, Kazakhstan

[4]Nuclear Research Department, Innovation and Digital Development Agency, Baku, Azerbaijan

[5]Institute of Physics Under Ministry of Science and Education, Baku, Azerbaijan

[6]Azerbaijan University of Architecture and Construction, Baku, Azerbaijan

E-mail: sidorova@jinr.ru

DOI: **10.32523/ejpfm.2026100202**
Received: 02.04.2026 - after revision

In experiments performed at GELINA (IRMM, Belgium) and IREN (FLNP JINR, Dubna, Russia) facilities, variations in the total kinetic energy (TKE) of fission fragments as a function of incident neutron energy were experimentally observed in the resonance region of $^{235}$U fission. These observations provided a basis to assume a correlation between the number of prompt fission neutrons and the TKE. To further investigate this dependence, the ENGREN setup was developed. It consists of a twin Frisch-gridded ionization chamber (GIC) with a target at its center, surrounded by 32 detectors based on EJ-309 liquid scintillator arranged in a spherical configuration around the GIC. The setup is designed for simultaneous measurement of the TKE and angular distributions of fission fragments, as well as for registration of prompt fission neutrons. We present its comprehensive calibration and performance validation. Energy calibration was performed by comparing measured gamma-ray spectra ( $^{22}$Na, $^{137}$Cs, $^{60}$Co) with Monte Carlo simulations, establishing a linear response ( $R^2 = 0.9977$ ) and an energy resolution of $\Delta E/E = 7.7\%$ at 1.333 MeV. The resolution parameters are consistent with the characteristics of organic liquid scintillators. Optimal neutron-gamma pulse shape discrimination (PSD) was achieved,

with Figure of Merit (FoM) values matching standard specifications. The system's readiness is demonstrated by a geometric efficiency of 4.55% and successful test measurements with a $^{235}$U target at the JINR IREN facility, confirming its capability for high-statistics fission studies.

**Keywords:** double ionization chamber; nuclear fission; fission fragments; total kinetic energy; prompt fission neutrons; mass distribution; liquid scintillation detectors

# Introduction

Investigation of the properties of prompt fission neutrons (PFN) plays a key role in studying the fundamental characteristics of the nuclear fission process. PFNs are emitted at the moment of heavy nucleus splitting and contain important information about the configuration and excitation degree of the fissioning nucleus at the scission point [1–4]. Understanding the distributions of neutron energy, emission direction, and time allows refining models of nuclear dynamics and contributes to solving applied problems – from reactor physics to nuclear safety.

Particular attention is drawn to possible correlations between the PFN yield and the total kinetic energy (TKE) of fission fragments. In an experiment performed at the GELINA accelerator (IRMM, Belgium), TKE variations depending on the incident neutron energy in the resonance region were experimentally observed for the first time in $^{235}$U fission [5]: with a change in the incident neutron energy on the order of an eV, the TKE variation amounted to hundreds of keV (Figure 1).

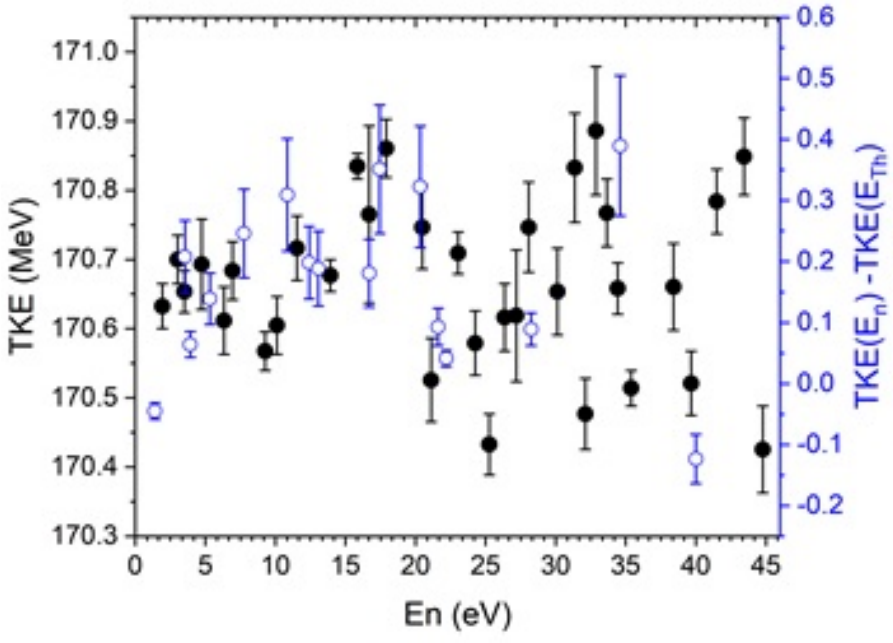


Figure 1. Total kinetic energy (TKE) of fission fragments from $^{235}$U(n,f) as a function of incident neutron energy. Black symbols: data from GELINA (IRMM, Belgium) [5]; blue symbols: data from IREN (JINR, Dubna, Russia) [6].

Independent confirmation of the observed variations was obtained at the Neutron Physics Laboratory of the Joint Institute for Nuclear Research (JINR), where similar measurements were carried out at the IBR-30 facility using the IREN resonant neutron source [6]. Thus, the observed effects were reproduced in a different experimental environment, which increases their significance and

reliability. It was assumed that prompt fission neutrons play a significant role in this process; however, the data obtained suffered from insufficient statistics to confirm this assumption. This motivated the development of a multi-module setup for PFN registration. At the FLNP JINR, the ENGREN setup was developed, designed for more efficient registration of neutrons and associated parameters of fission events.

## Experimental Setup

A photograph of the experimental setup is presented in Figure 2, displaying the geometrical configuration of the scintillation array and the placement of the ionization chamber. Structurally, it consists of a twin ionization chamber with Frisch grids and a target located at the center, as well as a PFN detection system comprising 32 detector modules positioned on an imaginary spherical surface with a radius of 500 mm around the target center.

The twin ionization chamber with Frisch grids is formed by two ionization chambers separated by a common cathode. The target, 70 mm in diameter, is located directly on the common cathode. In each chamber, the anode is positioned at a distance of 200 mm from the cathode. Between the anode and the cathode, at a distance of 20 mm from the anode, there is a Frisch grid designed to shield the anode from induced signals arising in the gap between the cathode and the grid. The chamber is filled with P10 gas mixture flowing at a rate of 20 ml/min under normal conditions. The target can be made of fissile materials ($^{235}$U, $^{237}$Np, $^{239}$Pu), for which PFN emission is initiated by neutron-induced fission, as well as $^{252}$Cf, for which spontaneous fission is registered. When a target nucleus undergoes fission, the resulting fission fragments fly apart in opposite directions and enter the different chambers of the twin ionization chamber. Moving through the gaseous medium, the fission fragments ionize its atoms, creating electrons and positive ions. Under the influence of the electric field, electrons drift toward the anode, while positive ions drift toward the cathode. The motion of electrons induces a signal on the cathode, which is used as the event start time stamp. The contribution of electrons to the anode signal becomes significant only after they pass through the Frisch grid. Due to the shielding properties of the grid, the anode records a signal proportional to the particle's energy, without influence from processes occurring in the region between the cathode and the grid. For each fission event, the twin ionization chamber records the following information:

- event time stamp (from the cathode signal);
- emission angles of FF relative to the laboratory coordinate system;
- pulse heights (energies) of FF (from the anode signals).

The detector modules are arranged on four sections of a virtual spherical surface with a radius of 50 cm: 12 modules are located on two sections with a diameter of 300 mm, and the remaining 20 modules are on two sections with a diameter of 450 mm. This arrangement of 32 detectors on a sphere with a radius

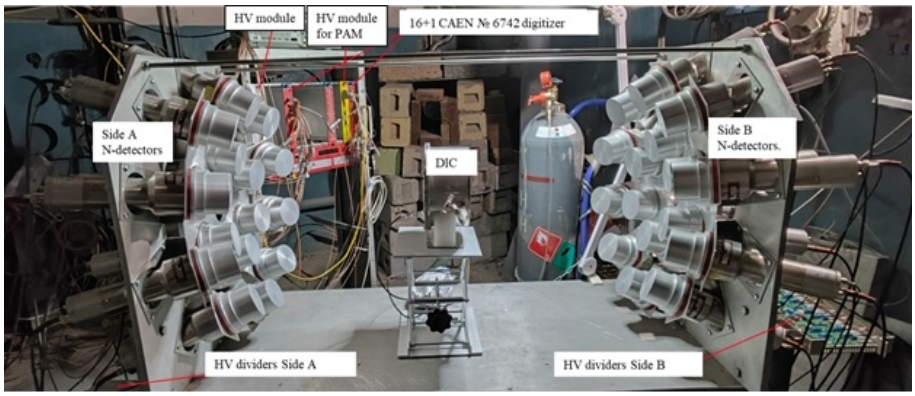


Figure 2. Photograph of the ENGREN experimental setup, showing the symmetrical arrangement of 32 EJ-309 liquid scintillators around the central fission ionization chamber.

of 50 cm results in a total geometric efficiency of approximately 4.55% of $4\pi$, corresponding to a solid angle of 0.5713 sr. Each PFN detection module is an aluminum cylinder 76 mm in diameter and 51 mm high with a wall thickness of 3 mm, filled with EJ-309 liquid scintillator. A photomultiplier tube (PMT), optically coupled to the transparent end face of the cylinder, serves to amplify the light flashes produced when PFN interact with the scintillator molecules.

Specialized software has been developed to study the properties of PFN recorded using the new system, which includes detectors, electronic data acquisition equipment, and data acquisition and analysis software. Pulses caused by PFN are amplified by the PMTs and analyzed by the data acquisition system to separate PFN from background gamma radiation using the pulse shape discrimination method. A pulse is recorded by the data acquisition system when it exceeds a set amplitude threshold.

## Calibration and Signal Processing Methodology

The initial tests focused on evaluating and optimizing the performance of the scintillation detectors within the ENGREN experimental setup. This process involved calibrating the liquid scintillation detectors for accurate neutron detection and developing effective methods for neutron-gamma separation using pulse shape discrimination. Signal acquisition was performed using CAEN digitizers, model N6742, based on the DRS4 chip with 12-bit resolution and a sampling rate of up to 5 GS/s, enabling high-precision readout of the photomultiplier pulse shapes. A connection scheme between the detectors, digitizers, and the data acquisition PC was implemented for system integration and testing. To expand the system's capabilities, DSR-32 digitizers developed at JINR (32 channels, 200 MHz, 11 bit), controlled by Romana software (TANGRA project) [7], were also used and tested. Prior to the setup's construction, the systematic error associated with crosstalk between detectors in the multichannel recording system was estimated using the Monte Carlo method. This estimation showed that the level of neutron crosstalk does not exceed 5% [8]. Accurate neutron-gamma discrimination is essential for reducing background noise and improving measurement accuracy. As part of the setup validation, the optimal operating voltage for each scintillation detector

was determined. Although the detectors underwent factory testing prior to delivery, additional verification was performed using a $^{60}$Co gamma source to ensure operational stability under experimental conditions. The results showed that while most detectors exhibited similar operating voltages, several detectors deviated significantly from the average value, indicating the need for individual calibration. Figure 3 (left) shows the operating voltages obtained for all detectors, grouped by their position to the left and right of the ionization chamber.

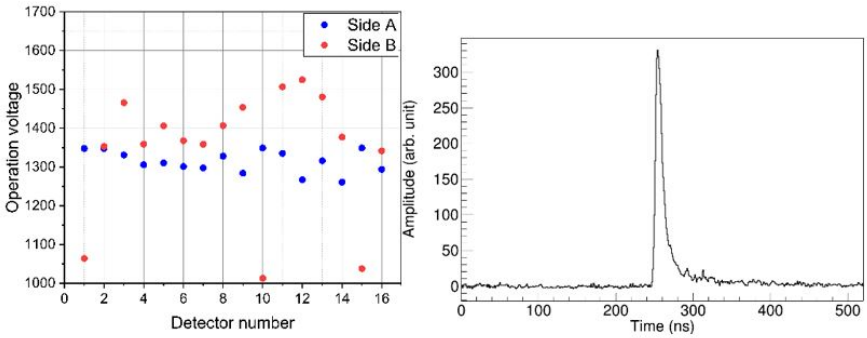


Figure 3. Operating voltage as a function of detector number (left) and the recorded pulse shape from a liquid scintillator detector when irradiated with a $^{60}$Co source (right).

To evaluate detector performance and analyze pulse parameters, digital signal processing was applied. Pulse amplitude analysis, in particular, served as a diagnostic tool to verify the operational status of each detector. Variations in pulse amplitude can indicate deviations in PMT gain, signal attenuation, or incorrect trigger settings. Figure 4 shows the pulse amplitude spectra for 16 detectors irradiated with a $^{60}$Co gamma source and a Pu-Be neutron source. Due to the interaction mechanisms of gamma quanta in the scintillator, the observed spectra mainly represent Compton electrons, which dominate the signal in this energy range. The pulse amplitude spectra for all detectors are nearly identical, as shown in Figure 4, indicating that uniform gain has been achieved across all detectors.

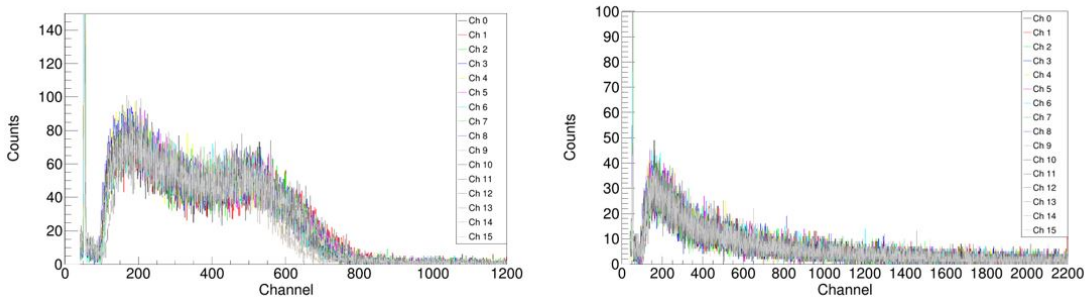


Figure 4. Pulse amplitude spectra from a $^{60}$Co gamma source (left) and a Pu-Be neutron source (right) recorded by 16 detector.

Figure 5 presents the results of neutron-gamma discrimination using the charge integration method for both types of sources. As expected, the spectrum from $^{60}$Co (left) shows a single gamma band, while the spectrum from Pu-Be (right) exhibits distinct neutron and gamma bands. Using the gamma source (Figure 5, left) instead of the neutron source (Figure 5, right) yielded the expected result – only background neutrons were registered.

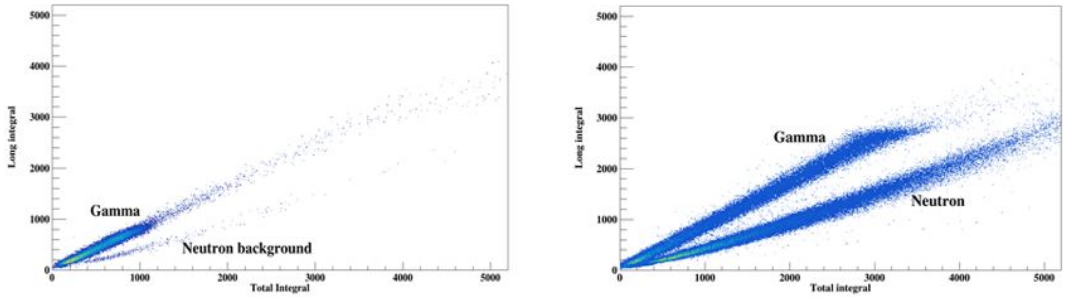


Figure 5. Results of neutron-gamma ( $n$ - $\gamma$ ) discrimination using the charge integration method for $^{60}$ Co (left) and Pu-Be (right) sources.

Figure 6 (left) presents the long-to-total (L/T) integral ratio for $^{60}$ Co (black) and Pu-Be (red). The first peak corresponds to neutrons, and the second to gamma rays. As can be seen, the gamma peaks from $^{60}$ Co and Pu-Be coincide in position. The corresponding peaks were fitted with a Gaussian function to accurately determine their centers. To determine the operating voltage for each detector at which the best separation of neutrons and gamma rays is achieved, a standard quantitative metric – the Figure of Merit (FoM) – was used, calculated from the short-to-long (S/L) integral ratio histograms using the formula:

$$\text{FoM} = \frac{D}{\text{FWHM}_n + \text{FWHM}_\gamma} \tag{1}$$

where $D$ is the distance between the neutron and gamma peak centers, $\text{FWHM}_n$ and $\text{FWHM}_\gamma$ are their full widths at half maximum. To achieve optimal neutron-gamma separation, the integration time windows were optimized for each detector as a function of bias voltage. The optimization parameters were: $t_1$ – delay of the integration start relative to the trigger threshold; $t_2$ – end of the short integration interval; $t_3$ – end of the long integration interval. For each detector and bias voltage, the combination of $t_1$, $t_2$ and $t_3$ that maximized FoM was determined. For each detector and each bias voltage, the maximum FoM value was determined. The optimal operating voltage for each detector was then selected based on the highest FoM achieved. Figure 6 (right) presents, for each detector, the optimal bias voltage and the corresponding FoM value.

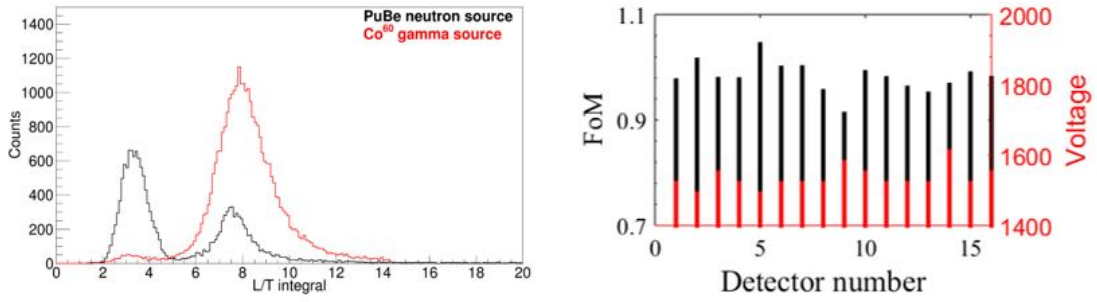


Figure 6. Long-to-total (L/T) ratio for gamma and neutron sources (left); Maximum FoM values and optimal operating voltages achieved for each detector (right).

# Modeling the response of the ENGREN detectors

Experimental spectra were measured using calibrated gamma sources: $^{22}$Na, $^{137}$Cs, and $^{60}$Co, covering the energy range from 0.511 MeV to 1.333 MeV. Room background was subtracted from the experimental spectra. Since the EJ-309 liquid scintillator consists of light elements (hydrogen and carbon) characterized by a small photoelectric cross-section, photopeaks in the experimental spectra are weakly pronounced and unsuitable for energy calibration.

The main interaction mechanism of monoenergetic photon radiation with the scintillator material in the energy range under consideration is Compton scattering. The energy transferred to an electron as a function of the scattering angle is given by the Compton formula (2):

$$E_e = \frac{E_\gamma^2(1-\cos\theta)}{m_e c^2 + E_\gamma(1-\cos\theta)} \tag{2}$$

where $E_e$ – energy transferred to the recoil electron; $E_\gamma$ – incident gamma-ray energy; $\theta$ – scattering angle of the gamma photon; $m_e c^2 = 0.511$ MeV – electron rest energy.

Its upper boundary, the Compton edge (ECE), corresponds to the maximum energy transfer occurring at backscattering ($\theta = 180^\circ$):

$$E_{\mathrm{CE}} = \frac{2E_\gamma^2}{m_e c^2 + 2E_\gamma} \tag{3}$$

The Compton edge values $E_{\mathrm{CE}}$ (3) used for the calibration sources are given in Table 1. The emission probabilities for the specified isotopes (see Table 1) were taken from [9]. Based on these data, the relative intensities of radiation at different energies were calculated for each isotope whose spectrum contains multiple energy components. These relative intensities were then used as weighting factors in the simulation of electron energy spectra for each isotope.

Table 1.
Parameters of gamma sources and energy resolution obtained by fitting a Gaussian convolved with Monte Carlo results.

| Isotope | Gamma-ray Energy $E_\gamma$ (MeV) | Compton Edge Position $E_{\mathrm{CE}}$ (MeV) | Emission probability ($\gamma$/decay) | $\sigma$ (MeV) | $\Delta E/E$ |
|---|---|---|---|---|---|
| $^{22}$Na | 0.511 | 0.341 | 1.798 | 0.0474 | 0.1391 |
| $^{22}$Na | 1.273 | 1.062 | 0.9994 | 0.0535 | 0.1120 |
| $^{137}$Cs | 0.662 | 0.478 | 0.851 | 0.0799 | 0.0830 |
| $^{60}$Co | 1.173 | 0.963 | 0.9985 | 0.0828 | 0.0780 |
| $^{60}$Co | 1.333 | 1.118 | 0.999826 | 0.0858 | 0.0767 |

The position of the Compton edge $E_{\mathrm{CE}}$ is determined by kinematics, while the shape of the spectrum and the observed position of the Compton peak depend on the detector's energy resolution. To model the detector response, a specialized program was developed implementing the Monte Carlo method for direct tracking of photons.

The simulation includes Compton scattering and photoelectric absorption, which are the dominant interaction mechanisms in the EJ-309 scintillator for the energies considered in this work (up to 1.3 MeV from $^{60}$Co sources). EJ-309 is an organic liquid scintillator with a chemical composition based on hydrocarbons,

consisting primarily of hydrogen and carbon atoms [10]. According to the manufacturer's specifications, the number of hydrogen atoms is $5.43 \times 10^{22}$ per $\mathrm{cm}^3$ and carbon atoms is $4.35 \times 10^{22}$ per $\mathrm{cm}^3$, with a density of $0.959\ \mathrm{g/cm^3}$. Pair production, while kinematically possible above 1.022 MeV, has a negligible contribution in this energy region for organic scintillators due to their low atomic number $Z$ – the pair production cross section scales approximately as $Z^2$, making it significant only in high-$Z$ materials. According to the NIST XCOM database [11], for carbon ($Z = 6$) and hydrogen ($Z = 1$) at 1.3 MeV, the pair production cross section is more than three orders of magnitude smaller than the Compton scattering cross section. Therefore, pair production was omitted from the simulation. The simulation performs complete, event-by-event tracking of photons throughout the entire geometry of the setup, including the aluminum detector housings, without any simplifications or artificial cutoffs. All relevant physical processes are included: photons undergo multiple Compton scattering, lose energy progressively, and may produce secondary photons that are themselves tracked. Energy deposited in the aluminum housing is considered lost and does not contribute to the detector response, as it does not reach the photomultiplier tube. A photon history terminates either when the photon escapes the setup entirely or when it is absorbed via the photoelectric effect, which becomes increasingly probable as the photon energy degrades. The resulting energy deposition spectra correspond to an ideal detector with infinite energy resolution, reflecting only the underlying physical processes such as multiple Compton scattering.

To validate the core algorithm, benchmark simulations were performed against the well-established GEANT4 toolkit [12] for a single EJ-309 detector. In this simulation-based comparison, the detector, with a diameter of 50.8 mm and a length of 50.8 mm, has an aluminum housing 1 mm thick and is filled with EJ-309 liquid scintillator. A 22-mm diameter source was positioned 10 mm from the detector surface, with photons incident parallel to the detector axis. A comparison between the reference spectrum generated by GEANT4 and the spectrum obtained with our code is shown in Figure 7, demonstrating excellent agreement between the two simulations.

Using the geometric data of our setup and source parameters, the Compton electron spectra from the calibration sources $^{22}$Na, $^{137}$Cs, and $^{60}$Co were calculated with the developed Monte Carlo program.

## Energy Calibration

The Klein–Nishina formula describes the energy distribution of electrons from a single Compton scattering event. However, multiple subsequent interactions within the detector volume distort this initial distribution, transforming the sharp Compton edge $E_{\mathrm{CE}}$ into a broader structure – even in the case of an ideal detector with infinite energy resolution. For calibration purposes, the most prominent feature of this structure, referred to as the simulated Compton peak at energy $E_C$, was fitted with a Gaussian function to determine its centroid. The same fitting

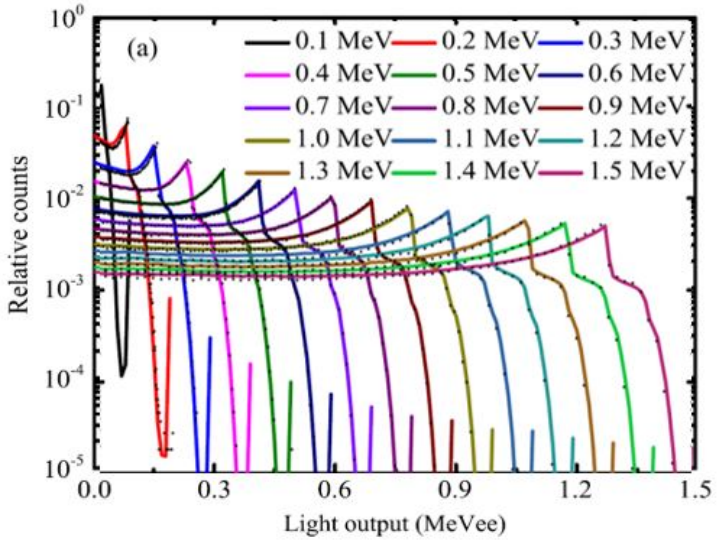


Figure 7. Comparison of the Compton electron spectra simulated using the GEANT4 package [11] and those obtained with the in-house developed code (indicated by black points).

procedure was applied to the experimental spectra to extract the corresponding peak positions $P_C$ (in ADC channels). These experimental values were then plotted against the simulated peak positions and fitted with a linear function.

As shown in Figure 8 (left), the calibration is linear over the entire energy range under study, coefficient of determination $R^2 = 0.9977$. Approximation of the experimental points with the linear function

$$P_C = G(E_C - E_0) \tag{4}$$

yielded parameter values $G = 0.0503$ channels/MeV and $E_0 = 0.031$ MeV. The obtained parameters are physically justified and agree well with the expected behavior of liquid organic scintillators.

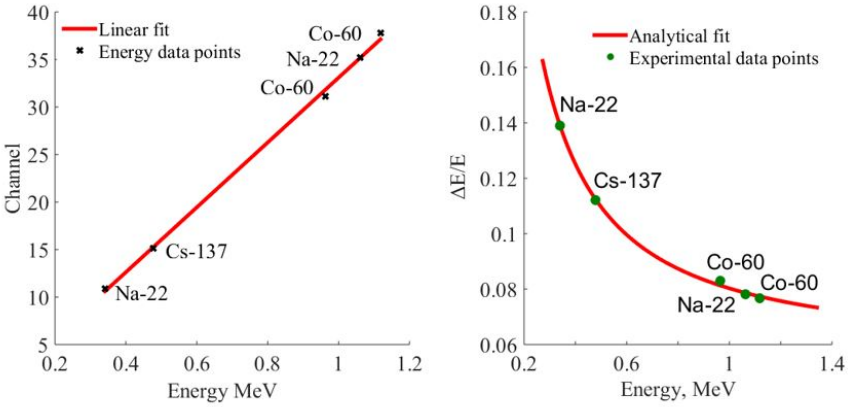


Figure 8. Left: Energy calibration of the EJ-309 liquid scintillator. The position of the Compton edge (in ADC channels) for $^{22}$Na, $^{137}$Cs, and $^{60}$Co sources is plotted against the electron-equivalent energy. Crosses represent experimental data points; red line is a linear fit using Eq. (4). Right: Relative energy resolution $\Delta E/E$ as a function of electron-equivalent energy. Green points are the resolution values obtained from fitting the experimental data with a convolution of Monte Carlo simulated spectra and a Gaussian function. The red solid line is a fit using the analytical function from Eq. (5).

## Energy Resolution

After fixing the energy calibration parameters, the procedure for determining the resolution was performed for each calibration source. The model spectra, initially calculated by the Monte Carlo method in the electron-equivalent energy scale, were converted to the ADC channel scale using the obtained calibration parameters $G$ and $E_0$. The experimental spectrum was then fitted with a convolution of the corresponding model spectrum (now in channel space) and a Gaussian function representing the detector energy resolution (Figure 9). The standard deviation $\sigma$ of the Gaussian served as a free fitting parameter and characterized the energy resolution of the detector at the energy corresponding to the given calibration source.

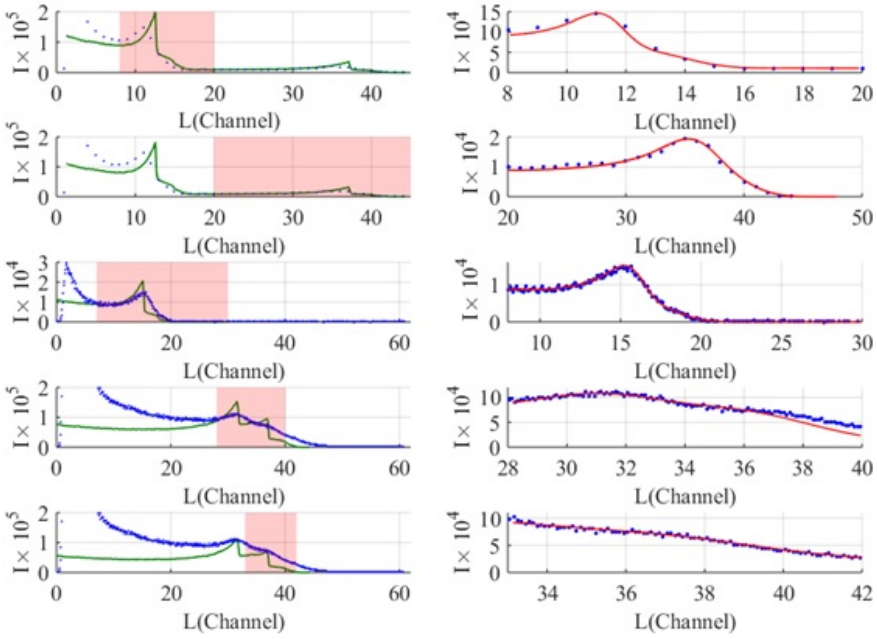


Figure 9. Energy spectra of Compton electrons from calibration sources. The y-axis shows intensity $I$ (scaled by the factor indicated on each plot). Blue points represent experimental data, and the green line shows the Monte Carlo simulation. The pink shaded areas indicate the fitting regions. The left panels show the full energy range, while the rightmost panel displays a zoomed-in view of the fitting region. In the zoomed panel, the red line represents the convolution of the simulation with a Gaussian function: (a–b) $^{22}$ Na; (c) $^{137}$ Cs; (d–e) $^{60}$ Co.

The relative energy resolution $\Delta E/E$ was calculated for the calibration monoenergetic photons: $\Delta E/E_{^{22}\mathrm{Na}}(0.511\ \mathrm{MeV}) = 0.1391$, $\Delta E/E_{^{137}\mathrm{Cs}} = 0.1120$, $\Delta E/E_{^{60}\mathrm{Co}}\ (1.173\ \mathrm{MeV}) = 0.0830$, $\Delta E/E_{^{22}\mathrm{Na}}\ (1.273\ \mathrm{MeV}) = 0.0780$, $\Delta E/E_{^{60}\mathrm{Co}}(1.333\ \mathrm{MeV}) = 0.0767$.

Both the absolute ($\sigma$) and relative ($\Delta E/E$) resolution values obtained from this procedure are summarized in Table 1. The experimental points were fitted with the analytical dependence commonly used for scintillation detectors [13]:

$$\frac{\Delta E}{E} = \sqrt{\alpha^2 + \frac{\beta^2}{E} + \frac{\gamma^2}{E^2}} \tag{5}$$

where $\alpha$ is the constant term related to light collection non-uniformities, $\beta$ represents statistical fluctuations in photoelectron production ($1/\sqrt{E}$ dependence), and $\gamma$ describes electronic noise ($1/E$ dependence). The fit, shown in Figure 8

(right), yields $\alpha = 0.0557 \pm 0.0090$, $\beta = 0.0472 \pm 0.0146$, $\gamma = 0.0335 \pm 0.005$ with $R^2 = 0.9987$. These values are characteristic of organic liquid scintillators.

It should be noted, however, that the $\beta$ and $\gamma$ parameters exhibit a strong correlation in the fit due to the limited number of data points and the absence of resolution measurements below 0.511 MeV. In this energy region, the $1/\sqrt{E}$ and $1/E$ functional forms are difficult to distinguish, which may lead to an overestimation of $\gamma$ and a corresponding underestimation of $\beta$. Consequently, the individual values of $\beta$ and $\gamma$ should be interpreted with caution, while their combined contribution to the energy resolution remains well constrained by the data.

## Validation of the system performance in detecting fission events

To test the entire system under simplified readout conditions, a fission experiment was conducted at the IREN neutron source [14, 15]. A thick $^{235}$U target was used with a simple ionization chamber, where signals were read out only from the cathode. The energy spectrum obtained in this configuration is shown in Figure 10.

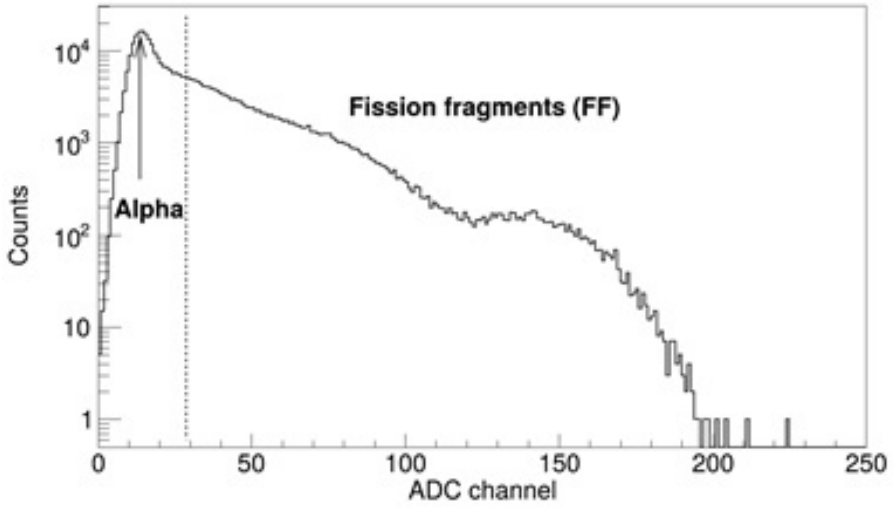


Figure 10. Pulse amplitude spectrum obtained from the fission ionization chamber with a thick uranium target using cathode-only signal readout.

The spectrum shows three distinct regions corresponding to different types of registered events. The sharp peak at low ADC channels corresponds to alpha particles from the natural decay of uranium isotopes, which deposit relatively little energy in the gas. This is followed by a broad, flat region in the middle ADC channels, representing events from fission fragments that deposit only part of their energy due to significant energy losses in the thick uranium layer or incomplete charge collection. This plateau is characteristic of operation with a thick target, where many fission fragments do not fully escape into the gas volume. At higher ADC channels, a broad peak is observed, corresponding to

full energy deposition from fission fragments that enter the gas with minimal losses, typically from fissions occurring near the uranium surface. The overall shape of the spectrum reflects the combined influence of the target thickness, the ionization chamber geometry, and the method of signal readout from the cathode only.

# Results and Discussion

## Detector Uniformity and Operational Stability

The initial verification of all 32 EJ-309 detectors using a $^{60}$Co source revealed variations in optimal operating voltages (Figure 3, left). While the majority of detectors clustered around a mean value, several exhibited deviations of 10–15%. This finding underscores an important practical consideration for multi-detector arrays: even detectors from the same production batch require individual characterization. Factory-provided specifications, while useful as guidelines, cannot replace direct measurement of each channel's response. Despite these voltage variations, the pulse amplitude spectra obtained from all detectors under $^{60}$Co and Pu-Be irradiation were nearly identical (Figure 4). This indicates that gain matching was successfully achieved across the array, a prerequisite for consistent detection efficiency in angular correlation measurements.

## Neutron-Gamma Discrimination Performance

Pulse shape discrimination using the charge integration method clearly resolved neutron and gamma bands in the Pu-Be spectrum, while the $^{60}$Co source produced only the expected gamma band (Figure 5). The long-to-total ratio distributions (Figure 6, left) show excellent alignment of the gamma peaks from both sources, confirming the stability of the PSD method across different radiation fields. The FoM was calculated from short-to-long histograms for each detector as a function of applied voltage and integration gate parameters. The obtained FoM values, shown in Figure 6 (right), fall within the range typical for organic liquid scintillators. This is an expected result, as the EJ-309 scintillator is well characterized in the literature, and our optimization procedure simply confirms that the detectors perform according to specifications. The variation in optimal voltages across detectors (Figure 6, right) demonstrates that detector-specific optimization is necessary; a universal setting applied to all channels would have resulted in suboptimal performance for some detectors. The optimized gate parameters are now established and ready for implementation in fission experiments.

## Energy Calibration

Energy calibration of liquid scintillators presents a well-known challenge due to the absence of distinct photopeaks. Our approach, comparing experimental Compton spectra with Monte Carlo simulations, addresses this limitation by providing objective, reproducible determination of Compton edge positions. The

calibration points obtained for $^{22}$Na, $^{137}$Cs, and $^{60}$Co exhibit excellent linearity ($R^2 = 0.9977$) over the 0.511–1.333 MeV range (Figure 8 (left)). The calibration parameters $G = 0.0503$ channels/MeV and $E_0 = 0.031$ MeV are consistent with the expected light yield characteristics of EJ-309 scintillators.

The agreement between our dedicated Monte Carlo code and GEANT4 simulations (Figure 7) validates the accuracy of the modeling approach. While GEANT4 remains the gold standard for detector simulations, a dedicated code offers practical advantages for systematic studies, including faster parameter sweeps and seamless integration with data analysis pipelines.

## Energy Resolution

Energy resolution was determined by fitting the experimental spectra with a convolution of the Monte Carlo simulated spectra and a Gaussian function for each calibration photon energy. The resolution values obtained at the isotope points range from 7.7% at 1.333 MeV to 13.9% at 0.511 MeV. These values were fitted with the analytical dependence commonly used for scintillation detectors (3). The fitting parameters obtained are $\alpha = 0.0557 \pm 0.0090$, $\beta = 0.0472 \pm 0.0146$, and $\gamma = 0.0335 \pm 0.0056$ (Figure 8 (right)). The fit provides an excellent description of the experimental data ($R^2 = 0.9987$), and the resulting parameter values are consistent with expectations for organic liquid scintillators.

The fitted value of $\gamma = 0.0335$ exceeds the range typically expected for electronic noise alone ($< 0.02$). However, this apparent excess is most likely an artifact of the fitting procedure rather than a genuine noise contribution. Because no calibration data were available below 0.511 MeV, the $(\beta/\sqrt{E})$ and $(\gamma/E)$ terms exhibit similar energy dependencies in the fitted region, leading to a strong correlation between the two parameters. The fit therefore redistributes part of the statistical variance into the noise term, inflating $\gamma$ while reducing $\beta$. The true electronic noise contribution, constrained by independent measurements of the baseline width, is estimated to be $\gamma < 0.02$ and does not significantly degrade the energy resolution. This interpretation is supported by the fact that the constant term $\alpha = 0.0557$, which is uncorrelated with $\gamma$ in this energy range, already provides a fully consistent description of the high-energy limit of the resolution.

## Fission Fragment Detection

The cathode-only fission spectrum obtained with the $^{235}$U target (Figure 10) exhibits the characteristic features expected from a thick fission target: a low-energy alpha peak from natural uranium decay, a plateau from partially deposited fission fragment energy, and a broad peak corresponding to full energy deposition of fragments escaping the target surface. This spectral shape confirms that the ENGREN array successfully registers fission events in coincidence with the ionization chamber, validating the data acquisition and synchronization systems.

It is important to note the limitations of this measurement. The thick target and simplified cathode-only readout preclude extraction of quantitative fragment

mass or energy distributions. The observed spectrum represents a convolution of fragment energy loss in the target, variable charge collection efficiency, and the detector response. However, for system validation purposes, this configuration serves its purpose: it demonstrates reliable fission event triggering and coincidence registration with the 32-detector array.

### Implications and limitations

The comprehensive characterization presented here confirms that the ENGREN system meets the design objectives for fission neutron spectrometry. The geometric efficiency of 4.55%, determined by the array configuration, combined with the validated PSD performance and energy calibration, positions the system for measurements with significantly improved statistics compared to previous studies [5, 6]. The FoM values, while not exceptional, are fully consistent with standard performance for this detector type and are sufficient for reliable neutron-gamma separation in fission experiments.

Several limitations of the current work should be acknowledged. First, the energy calibration was performed only up to 1.333 MeV ($^{60}$Co), while fission neutron spectra extend to several MeV. Extension to higher energies using monoenergetic neutron sources or tagged gamma sources would improve accuracy for fission measurements. Second, the cathode-only readout employed in the validation experiment limits the ability to correlate neutron emission with fragment properties. Third, the thick uranium target, while convenient for initial testing, introduces significant energy loss effects that complicate interpretation of fragment spectra. Fourth, the resolution fitting procedure would benefit from additional data points, particularly at lower energies, to better constrain the separation of statistical and noise contributions.

## Future Directions

Building on this characterization, several directions for future work are planned. Full anode–cathode readout of the ionization chamber will be implemented, enabling reconstruction of fragment masses and energies. Thin targets will be employed to minimize energy loss effects and improve fragment spectroscopy. The optimized discrimination parameters will be applied to measurements with $^{235}$U, $^{239}$Pu and other actinides to investigate isotope-dependent effects in prompt neutron emission.

The modular design of ENGREN also offers upgrade paths. Additional detector modules could be integrated to increase efficiency, and selected detectors could be replaced with alternative scintillators (e.g., stilbene) to optimize performance for specific energy ranges. The validated simulation framework developed in this work will guide such optimizations by predicting performance improvements before physical implementation.

# Conclusion

A new detector array, ENGREN, has been successfully developed and characterized for studying prompt neutron yields in resonance neutron-induced fission at the Joint Institute for Nuclear Research in Dubna, Russia. The system consists of 32 EJ-309 liquid scintillation detectors arranged in a spherical configuration around a double Frisch-gridded ionization chamber.

The comprehensive characterization performed in this work confirms that the ENGREN system is well-suited for advanced fission studies. Key achievements include:

Geometric efficiency of 4.55% (corresponding to a solid angle of 0.5713 sr), representing a significant improvement over a single-detector configuration (0.14%, 0.01785 sr) and providing the statistical power needed to address the limitations of previous studies [5, 6].

Energy calibration performed using $^{22}$Na, $^{137}$Cs, and $^{60}$Co sources demonstrated good linearity in the energy-channel relationship ($R^2 = 0.9977$) over the 0.511–1.333 MeV range. The calibration parameters $G = 0.0503$ channels/MeV and $E_0 = 0.031$ MeV are consistent with the expected light yield characteristics of EJ-309 scintillators.

Energy resolution was determined by fitting experimental spectra with the convolution of Monte Carlo simulations and a Gaussian function. The resolution values range from 7.7% at 1.333 MeV to 13.9% at 0.511 MeV. The fitted resolution parameters ($\alpha = 0.0557 \pm 0.0090$, $\beta = 0.0472 \pm 0.0146$, $\gamma = 0.0335 \pm 0.005$) are characteristic of organic liquid scintillators and provide an excellent empirical description of the resolution across the calibrated energy range ($R^2 = 0.9987$).

Neutron-gamma discrimination was optimized for each detector individually. A comprehensive PSD analysis was performed, and the efficiency of the PSD was studied as a function of operating voltage, allowing the optimal discrimination voltage to be determined for each detector. The obtained FoM values fall within the range typical for organic liquid scintillators, confirming that the detectors perform according to specifications. This optimization ensures maximum separation of neutrons and gamma rays, enhancing the reliability of the data.

Fission fragment detection was successfully demonstrated using a thick $^{235}$U target with cathode-only readout. The recorded pulse amplitude spectra exhibited characteristics determined by the target thickness, chamber geometry, and cathode-only signal readout, which is consistent with expectations for a thick uranium target. This confirms that the ENGREN array reliably registers fission events in coincidence with the ionization chamber, validating the data acquisition and synchronization systems.

The validated simulation framework, combining Monte Carlo calculations with analytical resolution modeling, provides a solid foundation for future systematic studies and detector optimizations. With its validated performance parameters, the ENGREN system is now ready to investigate correlations between prompt neutron emission and fission fragment properties. Future work will focus on implementing full anode-cathode readout, employing thin targets for improved fragment spectroscopy, and extending measurements to other actinides

including $^{239}$Pu.

## Acknowledgement

This project has received funding from the Science Committee of the Ministry of Science and Higher Education of the Republic of Kazakhstan (Grant no. BR31716181) and from Azerbaijan Science Foundation under grant agreement No [AEF-MGC-2024-2(50)-16/03/1-M-03].

## References

[1] H. Nifenecker et al., Nuclear Physics A **131** (1969) 261–266. [*CrossRef*]
[2] H.R. Bowman et al., Physical Review **126** (1962) 2120. [*CrossRef*]
[3] C. Budtz-Jorgensen, H.-H. Knitter, Nuclear Physics A **490** (1988) 307–328. [*CrossRef*]
[4] A. Al-Adili et al., Physical Review C **102** (2020) 064610. [*CrossRef*]
[5] Sh. Zeynalov et al., XII-ISINN. E3-2004-169, JINR (2004).[*Web Link*]
[6] Sh. Zeynalov et al., EPJ Web of Conferences **146** (2017) 04022. [*CrossRef*]
[7] I. Ruskov, Yu. Kopach, V. Bystritsky, EPJ Web of Conferences **256** (2021) 00014. [*CrossRef*]
[8] O. Sidorova, Sh. Zeynalov, Bulletin of the Russian Academy of Sciences: Physics **88** (2024) 1262–1266. [*CrossRef*]
[9] International Commission on Radiological Protection, Annals of the ICRP **38** (2008). [*CrossRef*]
[10] Eljen Technology, EJ-301, EJ-309 Data Sheet.[*Web Link*]
[11] M.J. Berger et al., XCOM: Photon Cross Sections Database, NIST Standard Reference Database 8 (XGAM), National Institute of Standards and Technology (2010).[*Web Link*]
[12] S. Zhang et al., Nuclear Instruments and Methods in Physics Research A **1006** (2021) 165407. [*CrossRef*]
[13] H. Klein, S. Neumann, Nuclear Instruments and Methods in Physics Research A **476** (2002) 132–142. [*CrossRef*]
[14] V. Shvetsov, Quantum Beam Science **1** (2017) 6. [*CrossRef*]
[15] S. Nuruyev et al., Nuclear Engineering and Technology **56** (2024) 1667–1671. [*CrossRef*]